JCI The Journal of Clinical Investigation

IRBIT governs epithelial secretion in mice by antagonizing the WNK/SPAK kinase pathway

Dongki Yang, … , Philip J. Thomas, Shmuel Muallem

J Clin Invest. 2011;121(3):956-965. https://doi.org/10.1172/JCI43475.

Research Article

Fluid and HCO_3^- secretion are fundamental functions of epithelia and determine bodily fluid volume and ionic composition, among other things. Secretion of ductal fluid and HCO_3^- in secretory glands is fueled by Na^+/HCO_3^- cotransport mediated by basolateral solute carrier family 4 member 4 (NBCe1-B) and by Cl^-/HCO_3^- exchange mediated by luminal solute carrier family 26, member 6 (Slc26a6) and CFTR. However, the mechanisms governing ductal secretion are not known. Here, we have shown that pancreatic ductal secretion in mice is suppressed by silencing of the NBCe1-B/CFTR activator inositol-1,4,5-trisphosphate (IP_3) receptor–binding protein released with IP_3 (IRBIT) and by inhibition of protein phosphatase 1 (PP1). In contrast, silencing the with-no-lysine (WNK) kinases and Ste20-related proline/alanine-rich kinase (SPAK) increased secretion. Molecular analysis revealed that the WNK kinases acted as scaffolds to recruit SPAK, which phosphorylated CFTR and NBCe1-B, reducing their cell surface expression. IRBIT opposed the effects of WNKs and SPAK by recruiting PP1 to the complex to dephosphorylate CFTR and NBCe1-B, restoring their cell surface expression, in addition to stimulating their activities. Silencing of SPAK and IRBIT in the same ducts rescued ductal secretion due to silencing of IRBIT alone. These findings stress the pivotal role of IRBIT in epithelial fluid and HCO_3^- secretion and provide a molecular mechanism by which IRBIT coordinates these processes. They also have implications for WNK/SPAK kinase–regulated […]

IRBIT governs epithelial secretion in mice by antagonizing the WNK/SPAK kinase pathway

Dongki Yang,[1,2] Qin Li,[2] Insuk So,[3] Chou-Long Huang,[4] Hideaki Ando,[5,6] Akihiro Mizutani,[5] George Seki,[7] Katsuhiko Mikoshiba,[5,6] Philip J. Thomas,[2] and Shmuel Muallem[1,2]

[1]The Epithelial Signaling and Transport Section, Molecular Physiology and Therapeutics Branch, National Institute of Dental and Craniofacial Research (NIDCR), NIH, Bethesda, Maryland, USA. [2]Department of Physiology, The University of Texas Southwestern Medical Center, Dallas, Texas, USA. [3]Department of Physiology and Biophysics, Seoul National University College of Medicine, Seoul, South Korea. [4]Department of Medicine and Division of Nephrology, The University of Texas Southwestern Medical Center, Dallas, Texas, USA. [5]Laboratory for Developmental Neurobiology, Brain Science Institute, Institute of Physical and Chemical Research (RIKEN), and [6]Calcium Oscillation Project, ICORP-SORST, JST, Wako, Saitama, Japan. [7]Department of Internal Medicine, Faculty of Medicine, University of Tokyo, Bunkyo-ku, Tokyo, Japan.

Fluid and HCO_3^- secretion are fundamental functions of epithelia and determine bodily fluid volume and ionic composition, among other things. Secretion of ductal fluid and HCO_3^- in secretory glands is fueled by Na^+/HCO_3^- cotransport mediated by basolateral solute carrier family 4 member 4 (NBCe1-B) and by Cl^-/HCO_3^- exchange mediated by luminal solute carrier family 26, member 6 (Slc26a6) and CFTR. However, the mechanisms governing ductal secretion are not known. Here, we have shown that pancreatic ductal secretion in mice is suppressed by silencing of the NBCe1-B/CFTR activator inositol-1,4,5-trisphosphate (IP_3) receptor–binding protein released with IP_3 (IRBIT) and by inhibition of protein phosphatase 1 (PP1). In contrast, silencing the with-no-lysine (WNK) kinases and Ste20-related proline/alanine-rich kinase (SPAK) increased secretion. Molecular analysis revealed that the WNK kinases acted as scaffolds to recruit SPAK, which phosphorylated CFTR and NBCe1-B, reducing their cell surface expression. IRBIT opposed the effects of WNKs and SPAK by recruiting PP1 to the complex to dephosphorylate CFTR and NBCe1-B, restoring their cell surface expression, in addition to stimulating their activities. Silencing of SPAK and IRBIT in the same ducts rescued ductal secretion due to silencing of IRBIT alone. These findings stress the pivotal role of IRBIT in epithelial fluid and HCO_3^- secretion and provide a molecular mechanism by which IRBIT coordinates these processes. They also have implications for WNK/SPAK kinase–regulated processes involved in systemic fluid homeostasis, hypertension, and cystic fibrosis.

Introduction

Transepithelial ion and HCO_3^- transport is the fundamental function of all epithelia and determines, among other things, bodily fluid volume and ionic composition, systemic and tissue acid-base balance and secretion, and absorption of ions and macromolecules. Numerous diseases are caused by aberrant epithelial function, depending on the altered transport or regulatory pathway. Na^+, K^+, Cl^-, and HCO_3^- transport by the gastrointestinal tract and the various segments of the renal tubule controls the absorption and secretion of these ions and thus systemic volume, blood pressure, and pH of biological fluids (1–3). The transport of these ions is determined by a hierarchy of transporters, including NKCC2, NCCT, KCCT, ENaC, ROMK, and Cl^- channels (3–5). Altered function of these transporters leads to unbalanced Na^+ and other ion homeostasis and thus hypo- or hypertension and hyperkalemia (3, 6). A major regulatory mechanism of all ion transporters is determination of their surface expression by the with-no-lysine (WNK) and the Ste20-related proline/alanine-rich kinase (SPAK) kinase pathways (3, 7).

The 4 members of the WNK kinase family (8) were discovered as homologs of MAP kinases (9), with WNK1, WNK3, and WNK4 regulating various Na^+, K^+, and Cl^- transporters (3, 7). The seminal discovery that mutations in WNK1 and WNK4 are associated with hypertension (10) led to extensive characterization of their function (3, 11). The kinase function of the WNKs is required for regulation of several transporters (3, 11). However, the WNKs have kinase-independent roles, also functioning as scaffolds (7). The most detailed information on the scaffolding function is available for WNK1 regulation of the K^+ channel ROMK (12–14), in which $WNK1^{1–119}$ upstream of the kinase domain mediates the full scaffolding function of WNK1 (14).

Several transporters are not regulated directly by the WNKs. Rather, the WNKs phosphorylate the sterile 20 kinase SPAK on T233 and other tyrosines (15), which acts on the transporters (7). $SPAK^{T233A}$ is kinase-dead ($SPAK^{KD}$) and acts to dominantly inhibit wild-type SPAK function. It is not known whether and how the WNK/SPAK pathway regulates secretory gland function. One goal of the present work was to define the mechanism by which the WNK/SPAK kinases regulate ductal fluid and HCO_3^- secretion using the pancreatic and parotid ducts as models.

Aberrant fluid and HCO_3^- secretion occurs in several epithelial diseases, including CF (16), pancreatitis (17), and Sjögren syndrome (18). The principal mechanism of HCO_3^- secretion is similar in many secretory epithelia. In the pancreatic and parotid ducts, about 70% of HCO_3^- enters the cells across the basolateral membrane (BLM) through the Na^+-HCO_3^- cotransporter identified as pNBC1 (19) (and renamed NBCe1-B; ref. 20), with the remaining 30% provided by the Na^+/H^+ exchanger NHE1 (1, 2, 4, 5). HCO_3^- exits the luminal membrane through the coordinated action of the Cl^- channel CFTR and the Cl^-/HCO_3^- exchanger SLC26 transporters, most commonly Slc26a6 and Slc26a3 (4).

Conflict of interest: The authors have declared that no conflict of interest exists.
Citation for this article: *J Clin Invest.* 2011;121(3):956–965. doi:10.1172/JCI43475.

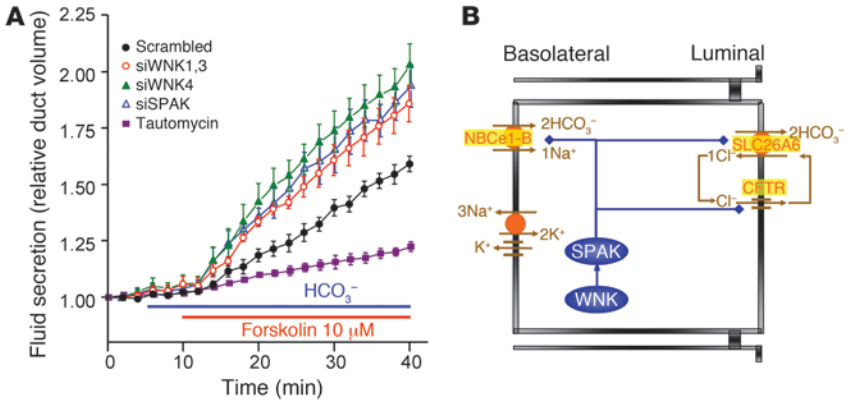

Figure 1

The WNK/SPAK and IRBIT/PP1 pathways in ductal fluid secretion. (**A**) Sealed pancreatic ducts in primary culture were treated with the indicated siRNA for 48–60 hours before measurement of stimulated ductal fluid secretion by video microscopy. Ducts treated with scrambled siRNA were also treated with the specific PP1 inhibitor tautomycin (3 nM). Similar inhibition of fluid secretion by tautomycin was observed with ducts not treated with scrambled siRNA. Secretion was initiated by incubation of the ducts in HCO_3^--buffered medium and stimulation with 10 μM forskolin. The traces are the mean ± SEM of 4–10 experiments. (**B**) Model of the main transporters determining ductal fluid secretion and how they may be regulated by the WNK/SPAK pathway.

Recently, we reported that ductal HCO_3^- secretion is coordinated by IRBIT (inositol-1,4,5-trisphosphate [IP_3] receptor–binding protein released with IP_3) (21). IRBIT was identified as a protein that competes with IP_3 for binding to the IP_3 receptors (22, 23). Subsequently, IRBIT was found to interact with and activate NBCe1-B (24). We showed that IRBIT has a central role in epithelial fluid and HCO_3^- secretion by activating both NBCe1-B in the BLM and CFTR in the luminal membrane (LM) of secretory gland ducts to stimulate fluid and HCO_3^- secretion (21). Activation of NBCe1-B (21, 24) and CFTR (21) occurs by direct interaction of IRBIT with the transporters and is dependent on the IRBIT PEST domain. These studies established IRBIT as the switch that triggers and sets the glands' fluid and HCO_3^- secretory state. Here, we asked what mechanism stabilizes the resting or inhibited state of the pancreatic and parotid ducts and examined the relationship between the events that inhibit secretion and IRBIT. We focused on the WNK kinases, since it was reported that they inhibit Slc26a6 (25, 26) and CFTR (27), although a recent study reported that WNK1 changes the HCO_3^- permeability of CFTR rather than inhibiting its activity (26). How the WNKs regulate the SLC26 transporters and CFTR is not known.

We report that the WNKs act through SPAK to suppress ductal fluid secretion, whereas IRBIT and PP1 markedly stimulate ductal fluid secretion and reverse the effect of the WNKs and SPAK. Detailed molecular analysis revealed that these effects are due to a reciprocal regulation of surface expression of the HCO_3^- transporters NBCe1-B and CFTR by the WNK/SPAK and by IRBIT/PP1 pathways. Most notably, in addition to direct activation of CFTR and NBCe1-B, IRBIT completely prevents the inhibitory effect of the WNKs and SPAK by recruiting PP1 to dephosphorylate the transporters that are phosphorylated by SPAK. These findings highlight the key role of IRBIT in controlling ductal fluid and HCO_3^- secretion and provide an inclusive molecular mechanism for coordination of epithelial fluid and electrolyte secretion.

Results

Role of the WNK and SPAK kinases in vivo. Previously we reported that IRBIT directly activates NBCe1-B (21, 24) and CFTR (21) to coordinate the stimulated state of fluid and HCO_3^- secretion by secretory ducts (21). On the other hand, nothing is known about the mechanisms that stabilize the physiologically important resting state, which is vital for the efficiency and fidelity of any physiological process. We reasoned that a potential pathway that stabilizes the resting state is the WNK/SPAK pathway, since WNK1 and WNK4 were reported to affect the activity of Slc26a6 (25) and CFTR expressed in *Xenopus* oocytes (27) and mammalian cells (26). To determine the role of the WNK and SPAK kinases in vivo, we used the approach of gene silencing by siRNA in sealed ducts in primary culture (28), which proved very efficient in these ducts (21, 29). The RT-PCR analysis in Supplemental Figure 1 (supplemental material available online with this article; doi:10.1172/JCI43475DS1) confirmed reports of expression of WNK1 and WNK4 in the pancreatic duct (10, 30) and revealed the expression of WNK3 in the duct. Similar findings were observed with the parotid duct (data not shown). Initially, we used an siRNA that efficiently knock down only WNK1 (data not shown). However, to minimize the need to apply multiple siRNA probes, we were able to design a single siRNA that knocked down both WNK1 and WNK3 (Supplemental Figure 1, B and C). Supplemental Figure 1, A and D, shows the efficiency of knockdown of WNK4 and of SPAK, respectively, in the pancreatic duct.

The siRNA probes were used to determine the role of the WNK and SPAK kinases in stimulated ductal fluid secretion. Figure 1A shows that silencing the *Wnk1* + *Wnk3*, *Wnk4*, and *SPAK* genes similarly increased the rate of ductal fluid secretion. Knockdown of *Wnk1* gave results similar to those obtained with knockdown of *Wnk1* + *Wnk3* (data not shown). Knockdown of all Wnks, *Wnk1* + *Wnk3* + *SPAK*, or of *Wnk4* + *SPAK* did not result in additive stimulation (data not shown), suggesting that the WNK and SPAK kinases function in the same pathway. The lack of additivity among the WNKs suggests that their activity is interdependent, as was found for WNK1 and WNK4 in the distal nephron (3, 31). The effect of the WNK and SPAK kinases on ductal secretion is opposite to that of IRBIT (21), which has a PP1-binding site (32). Indeed, inhibiting PP1 with tautomycin (33) markedly inhibited ductal secretion (Figure 1A), exactly as was found with knockdown of IRBIT (21).

Figure 1B depicts a molecular model that can explain the role of the WNK and SPAK kinases in pancreatic and salivary ductal secretion. In the model, the WNK kinases act on SPAK and SPAK inhibits the activity of the basolateral NBCe1-B and luminal CFTR and Slc26a6. SPAK phosphorylates the transporters to reduce their surface expression and thus their activity and consequently inhibits ductal secretion to stabilize the resting state. PP1 reverses the effect of SPAK. The results below provide comprehensive molecular dissection of this model and then reveal how IRBIT and PP1 regulate the function of the WNK/SPAK pathway.

Role of the WNK and SPAK kinases in ductal NBC activity. The key steps and transporters in ductal fluid and HCO_3^- secretion are

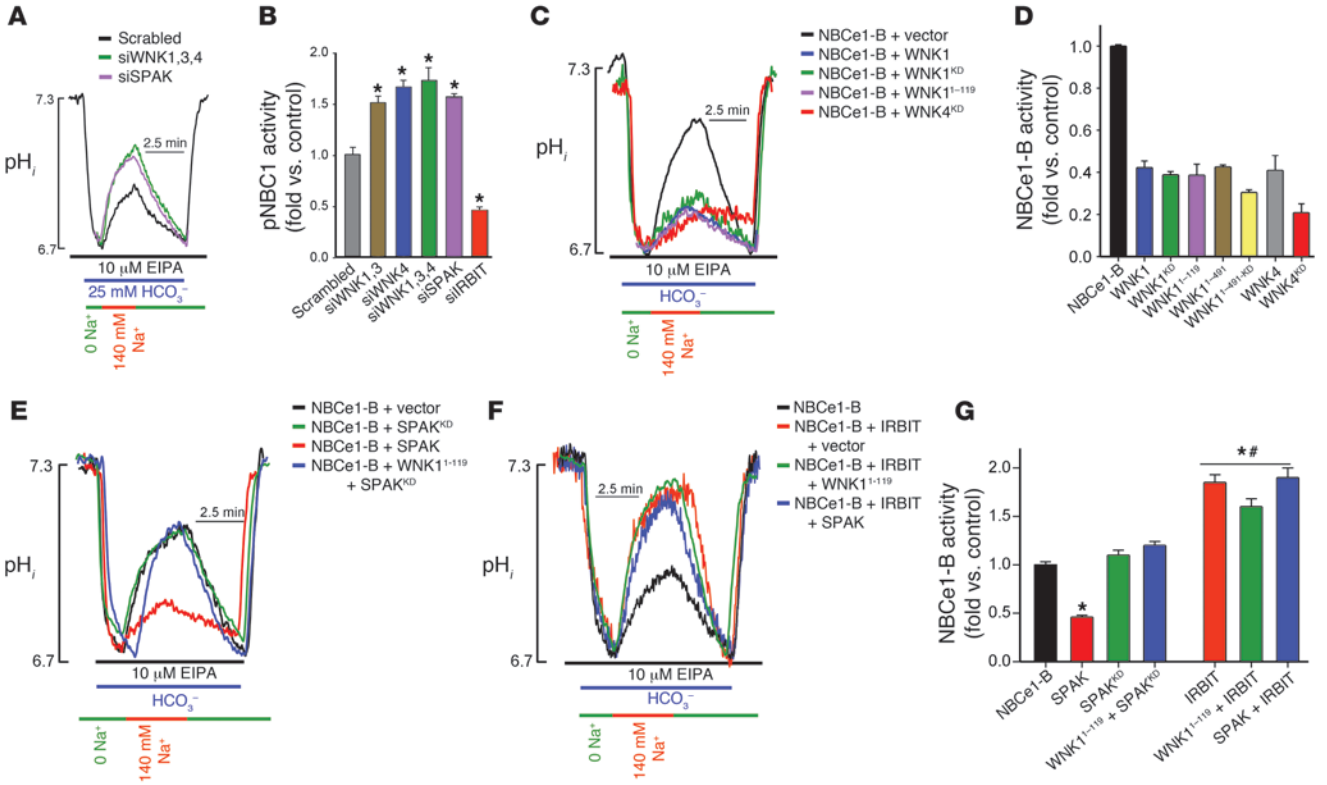

Figure 2

The WNK/SPAK pathway inhibits and IRBIT reverses inhibition of NBCe1-B activity. (**A** and **B**) Sealed pancreatic ducts treated with siRNA designed to knock down WNK1+WNK3 (siWNK1,3), WNK4, WNK1+WNK3+WNK4, and IRBIT were used to measure Na^+-HCO_3^- cotransport activity as the Na^+-dependent recovery from acid load in the presence of 10 μM EIPA. The results in **B** are the mean ± SEM of 3–8 ducts obtained from 3 separate mice; $^*P < 0.01$. (**C**–**G**) HeLa cells were transfected with NBCe1-B and either empty vector (black traces and first bar) or the indicated WNK, SPAK, and IRBIT constructs, and Na^+-HCO_3^- cotransport activity was measured. The bars show the mean ± SEM of 4–8 separate experiments (transfections), and for all conditions in **D**, $P < 0.001$ versus control. In **G**, $^*P < 0.01$ versus control; $^{\#}P < 0.001$ versus the condition without IRBIT.

Na^+-HCO_3^- cotransport–mediated (NBC-mediated) HCO_3^- entry by NBCe1-B across the BLM and CFTR-regulated and Slc26a6-mediated HCO_3^- exit across the luminal membrane (2, 21, 29, 34–36). Therefore, we determined the effect of depletion of the kinases on NBC and CFTR activities in the sealed ducts. NBC activity was measured as the Na^+-dependent and DIDS-inhibited recovery from acidification after treatment with *S*-(*N*-ethyl-*N*-isopropyl) amiloride (EIPA) to inhibit endogenous Na^+/H^+ exchangers (21). Figure 2, A and B, shows that depletion of individual and all 3 WNKs and of SPAK similarly increased ductal NBC activity by 50%–60%, while depletion of IRBIT inhibited ductal NBC activity. Regulation by WNKs and SPAK likely operates in several epithelia, since they are expressed in most epithelia. As an example, Supplemental Figure 2 shows regulation of NBC activity by IRBIT and the WNKs in sealed parotid duct. Parotid ducts seal after 12–24 hours in culture (37).

The WNK kinases act as scaffolds to inhibit NBCe1-B activity and surface expression. Expression of NBCe1-B and the WNK and SPAK kinases in model systems allows mapping of relevant domains and dissecting of the regulatory mechanism. As shown in Figure 2, C and D, we measured the effect of WNK1, WNK4, and various WNK constructs on the activity of NBCe1-B expressed in HeLa cells. Coexpression of WNK1 and WNK4 (and WNK3; data not shown) markedly inhibited NBCe1-B activity. The kinase function of the WNKs is not required for regulation of NBCe1-B, since the kinase-dead $WNK1^{D368A}$ ($WNK1^{KD}$) and $WNK4^{D318E}$ ($WNK4^{KD}$) inhibited NBCe1-B like the wild-type WNKs. Further analysis showed that $WNK1^{1–491}$, kinase-dead $WNK1^{1–491}$ ($WNK1^{1–491\text{-}KD}$), and $WNK1^{1–119}$ upstream of the kinase domain inhibit NBCe1-B like WNK1. These findings indicate that WNK1 functions as a scaffold, rather than a kinase, in the regulation of NBCe1-B.

In all cases examined, inhibition of ion transporters by the WNKs is due to reduced surface expression (3, 7, 11–13). Figure 3, A and B, shows that this is also the case for NBCe1-B, as $WNK1^{KD}$, $WNK4^{KD}$, $WNK1^{1–491}$, and $WNK1^{1–491\text{-}KD}$ all prominently reduce surface expression of NBCe1-B (WNK1 and WNK4 had similar effects; data not shown). Averages of 3–4 similar experiments and the *P* values for all experiments in Figure 3 are provided in Supplemental Figure 3.

SPAK mediates the function of the WNKs. The scaffolding function of the WNKs led us to ask whether their function is mediated by another kinase. Figure 2, E and G, shows that SPAK inhibited NBCe1-B activity, and Figure 3A shows that SPAK reduced surface expression of NBCe1-B, just like the WNKs. One mechanism by which the WNKs activate SPAK is phosphorylation of $SPAK^{T233}$ (3, 7). However, this cannot be a mechanism by which SPAK mediates

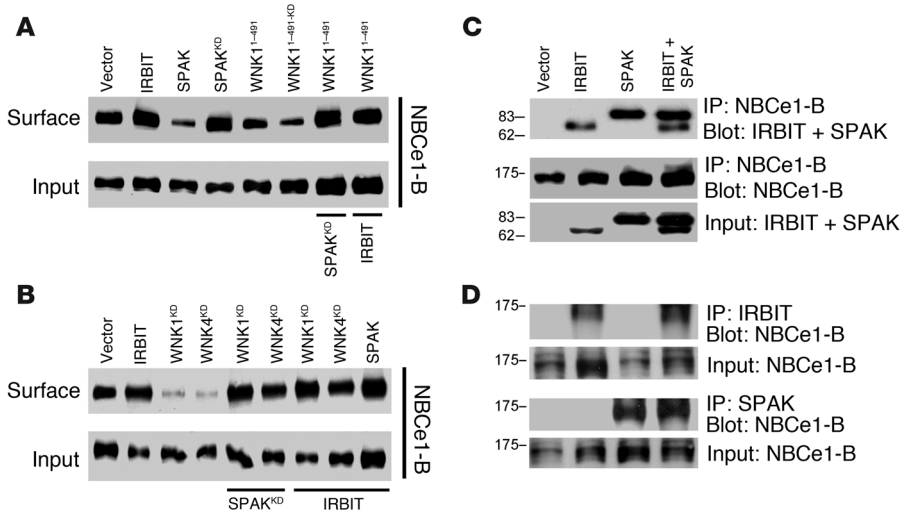

Figure 3

The WNK/SPAK pathway inhibits and IRBIT reverses inhibition of NBCe1-B surface expression without dissociating the NBCe1-B–SPAK complex. (**A** and **B**) HEK cells were transfected with GFP–NBCe1-B and the indicated WNK and Flag-SPAK constructs. Note that in the last two lanes in **A**, WNK1$^{1–491}$ was coexpressed with SPAK^{KD} and with IRBIT; and in lanes 5, 6 and 7, 8 in **B**, WNK1^{KD} and WNK4^{KD} were coexpressed with Flag-SPAK^{KD} and Flag-IRBIT, respectively. In lane 9 Flag-SPAK was coexpressed with Flag-IRBIT. The cells were used to determine total (lower blots) and surface expression (upper blots) of GFP–NBCe1-B by biotinylation. (**C** and **D**) HEK cells were transfected with GFP–NBCe1-B and with empty vector, Flag-IRBIT, Flag-SPAK, or Flag-IRBIT+Flag-SPAK and were used to determine the effect of IRBIT and SPAK on their interaction with GFP–NBCe1-B by coimmunoprecipitation assays. Note that IRBIT and SPAK do not affect their mutual interaction with NBCe1-B. NBCe1-B was detected with anti-GFP and SPAK and IRBIT with anti-Flag antibodies. Analysis of multiple experiments and averages are given in Supplemental Figure 3.

the function of the WNKs, since the kinase activity of the WNKs is not required to regulate NBCe1-B (and CFTR; see below). Alternatively, SPAK has autophosphorylation activity that phosphorylates T243 and T247, resulting in inhibition of NKCC1 (15). We therefore asked whether the WNKs can still act through SPAK by testing the effect of the dominant negative, kinase-dead SPAK^{KD}. SPAK^{KD} had no effect of NBCe1-B activity (Figure 2E) or surface expression (Figure 3A) but, most notably, prevented the inhibitory effect of the WNKs on the activity (Figure 2E) and surface expression (Figure 3, A and B) of NBCe1-B. Figures 2 and 3 show only selected examples, but similar results were obtained with all WNK constructs.

The combined findings with SPAK and SPAK^{KD} indicate that the WNKs and SPAK function in the same pathway that regulates the surface expression and consequently the activity of NBCe1-B. SPAK is downstream of the WNKs, and recruitment of SPAK by the WNK scaffolds leads to inhibition of NBCe1-B. These findings provide evidence to support the inhibition of NBCe1-B represented by the blue lines in Figure 1B.

IRBIT governs the function of the WNK/SPAK pathway. Inhibition of NBCe1-B by the WNK/SPAK pathway (Figure 2) and its stimulation by IRBIT (21, 24) raised the question of the relationship between them. Remarkably, IRBIT completely inhibited the effect of WNK1$^{1–119}$ and SPAK and activated NBCe1-B to the same extent in the presence and absence of the inhibitors (Figure 2, F and G). IRBIT alone had a minimal effect on surface expression of NBCe1-B (Figure 3, A and B). Yet IRBIT completely restored surface expression of NBCe1-B in the presence of WNK1$^{1–491}$, WNK1^{KD}, and WNK4^{KD}. Importantly, IRBIT also prevented reduction of NBCe1-B surface expression by SPAK. The effect of IRBIT was not due to preventing interaction of SPAK with NBCe1-B. Figure 3, C and D, shows that when SPAK and IRBIT were individually expressed with NBCe1-B, immunoprecipitation of NBCe1-B coimmunoprecipitated IRBIT and SPAK. Importantly, the same amount of SPAK and IRBIT immunoprecipitated with NBCe1-B when all proteins were expressed together and regardless of whether IRBIT, SPAK, or NBCe1-B were immunoprecipitated. Hence, IRBIT inhibits the effect of SPAK on NBCe1-B by a mechanism different from dissociation of the SPAK–NBCe1-B complex.

The results in Figures 2 and 3 and our previous findings (21, 24) indicate that IRBIT regulates the activity of NBCe1-B by two independent mechanisms. IRBIT antagonizes the effect of the WNK/SPAK kinases to stabilize expression of NBCe1-B at the plasma membrane. IRBIT also directly activates NBCe1-B by interaction of the IRBIT PEST domain with the N-terminus inhibitory domain of NBCe1-B (24) to activate NBCe1-B (21, 24).

PP1 mediates the effect of IRBIT. IRBIT has a PP1-binding site (32), and thus a potential mechanism by which IRBIT can reverse the effect of SPAK is recruitment of PP1 to the SPAK–NBCe1-B complex to dephosphorylate NBCe1-B and increase its activity. This scenario predicts that inhibition of PP1 should increase the effect of SPAK to inhibit HCO_3^- transport and fluid secretion. Indeed, inhibition of PP1 with tautomycin inhibited ductal fluid secretion (Figure 1A). Accordingly, Figure 4, A and B, shows that tautomycin inhibited ductal NBC activity.

Next, we tested the role of PP1 in activation of NBCe1-B by IRBIT using multiple protocols and probes. Significantly, overexpression of PP1 alone activated NBCe1-B nearly as well as IRBIT (Figure 4, C and D), and coexpression of IRBIT and PP1 did not result in further activation of NBCe1-B (data not shown). Inhibition of the native PP1 with tautomycin and by expression of the specific PP1 inhibitor inhibitor-2 (38) inhibited NBCe1-B activity to the same extent as the WNK and SPAK kinases (Figure 4, C and D). Importantly, IRBIT still stimulated NBCe1-B inhibited either by tautomycin or inhibitor-2, revealing the PP1-independent activity of IRBIT. The PP1-dependent and PP1-independent effects of IRBIT could be most clearly demonstrated with the mutant IRBIT$^{I42F44/AA}$, in which the consensus I42 and F44 of the IRBIT PP1-binding site were mutated to inhibit PP1 binding (32). At expression levels comparable to IRBIT, IRBIT$^{I42F44/AA}$ did not activate NBCe1-B (Figure 4D). Increasing IRBIT$^{I42F44/AA}$ expression 3-fold to increase its interaction with NBCe1-B resulted in activation of NBCe1-B (Figure 4D). This is consistent with earlier reports showing that IRBIT interacts directly with the N-terminus of NBCe1-B to activate the transporter by removing the inhibitory

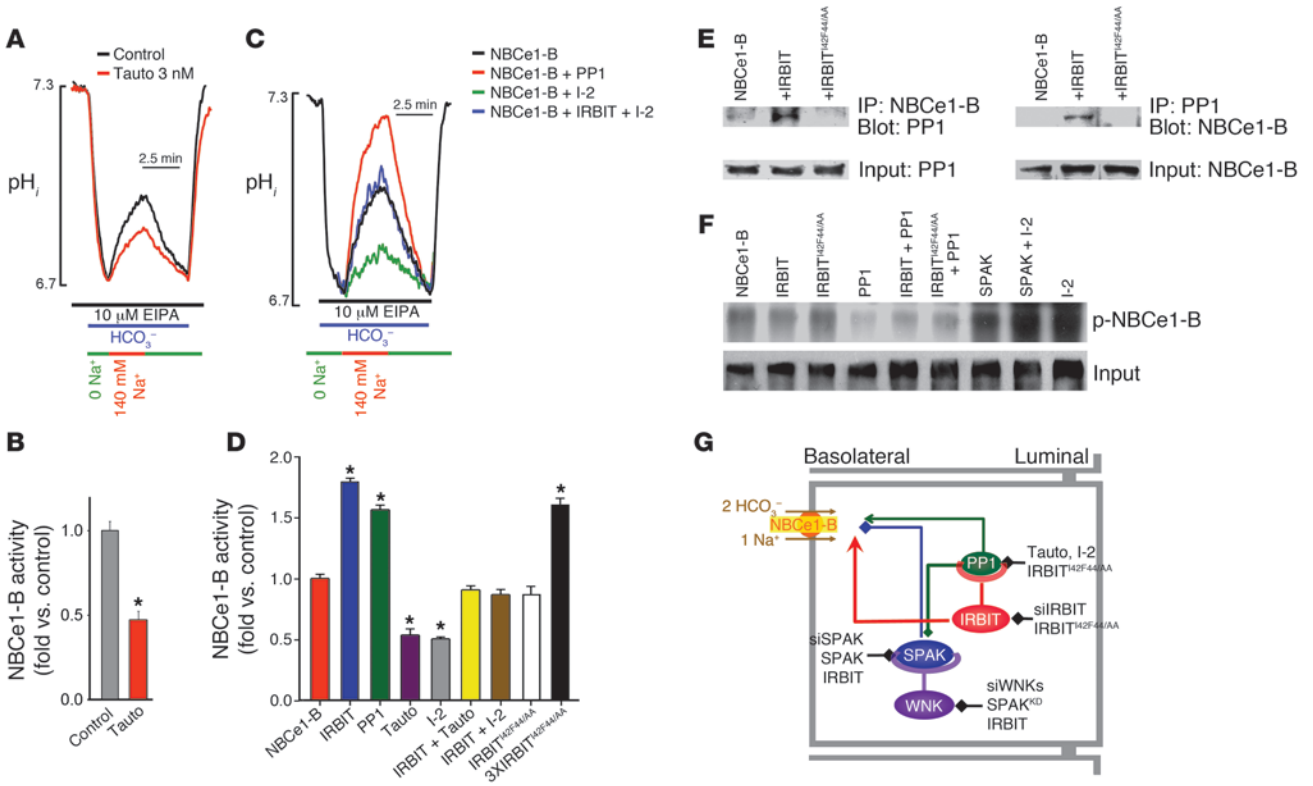

Figure 4

PP1 mediates all effects of IRBIT. (**A** and **B**) Sealed pancreatic ducts were treated with vehicle or with 3 nM tautomycin (Tauto) for 10 minutes, and Na^+-HCO_3^- cotransport activity was measured. **B** shows mean ± SEM (n = 3, *P < 0.001). (**C** and **D**) HeLa cells transfected with NBCe1-B and vector (black), PP1 (red), inhibitor-2 (I-2; green), or inhibitor-2 plus IRBIT (blue). Cells expressing NBCe1-B were also transfected with IRBIT (bars 2 and 6), $IRBIT^{I42F44/AA}$ (bar 8), and $3XIRBIT^{I42F44/AA}$ (bar 9) and treated with 3 nM tautomycin for 10 minutes (bars 4 and 6). **D** shows mean ± SEM of Na^+-HCO_3^- cotransport (n = 4–8, *P < 0.01). (**E**) HEK cells transfected with NBCe1-B and vector, IRBIT, or $IRBIT^{I42F44/AA}$ were used to test recruitment of the native PP1 to NBCe1-B. (**F**) HEK cells transfected with NBCe1-B and the indicated combinations of IRBIT, PP1, inhibitor-2, and SPAK constructs were labeled with ^{32}P for 2 hours. NBCe1-B was immunoprecipitated and NBCe1-B phosphorylation tested by radiography. (**G**) Model of regulation of NBCe1-B surface expression and activity by the WNK/SPAK and IRBIT/PP1 pathways and the relationship between them. The WNKs function as scaffolds for SPAK, which phosphorylates NBCe1-B to reduce its surface expression, and IRBIT functions as a scaffold for PP1, which dephosphorylates NBCe1-B to restore surface expression. IRBIT also activates NBCe1-B by preventing autoinhibition by NBCe1-B N-terminus. The black lines represent the probes used to test each component of the pathways. Averages for **E** and **F** are given in Supplemental Figure 4A and Supplemental Figure 5A, respectively.

effect of the N-terminus (24). A role of PP1 in the action of IRBIT implies that IRBIT recruits PP1 to NBCe1-B. The results in Figure 4E show that this is indeed the case, as IRBIT markedly increased coimmunoprecipitation of the native PP1 and NBCe1-B (n = 3, P < 0.01; see Supplemental Figure 3).

The multiple lines of evidence in Figure 4 suggest that IRBIT-recruited PP1 dephosphorylation of NBCe1-B antagonizes the phosphorylation of NBCe1-B by SPAK, which inhibits its localization to the cell surface and thus its activity. To provide direct evidence for this conclusion, we measured the effect of PP1, IRBIT, and SPAK on the phosphorylation of NBCe1-B in two assays. In Figure 4F cells transfected with the indicated constructs were labeled with ^{32}P, and phosphorylation of immunoprecipitated NBCe1-B was probed by radiography. In Supplemental Figure 5A, phosphorylation of immunoprecipitated NBCe1-B was probed by anti–phospho-serine/threonine antibodies. The figures show that IRBIT slightly reduced the phosphorylation of NBCe1-B, while the PP1-binding mutant $IRBIT^{I42F44/AA}$ did not. Expression of PP1 (alone or with IRBIT) nearly completely dephosphorylated NBCe1-B. On the other hand SPAK increased phosphorylation of NBCe1-B, as did expression of inhibitor-2, with maximal phosphorylation observed by expression of SPAK and inhibitor-2 (n = 3, P < 0.01).

Figure 4G summarizes the relationship between the WNK/SPAK kinases (blue) and the IRBIT/PP1 (green) pathways in regulating NBCe1-B expression and activity and the tools (black) used to probe each step. The resting inhibitory state is determined by the WNKs that function as scaffolds for SPAK. SPAK phosphorylates NBCe1-B to reduce its surface expression. IRBIT recruits PP1 to antagonize the action of the WNK/SPAK pathway to increase surface expression of NBCe1-B. IRBIT then directly activates NBCe1-B, determining the stimulated state of fluid and HCO3– secretion. The effect of PP1 is attributed to dephosphorylation of NBCe1-B by the phosphatase. However, it is possible that part of the effect of PP1 is due to dephosphorylation of SPAK by PP1. Recently, it was reported that PP1 dephosphorylates SPAK to partially reverse its stimulatory effect on NKCC1 activity (39). A similar process may contribute to the inhibitory effect of SPAK on NBCe1-B activity.

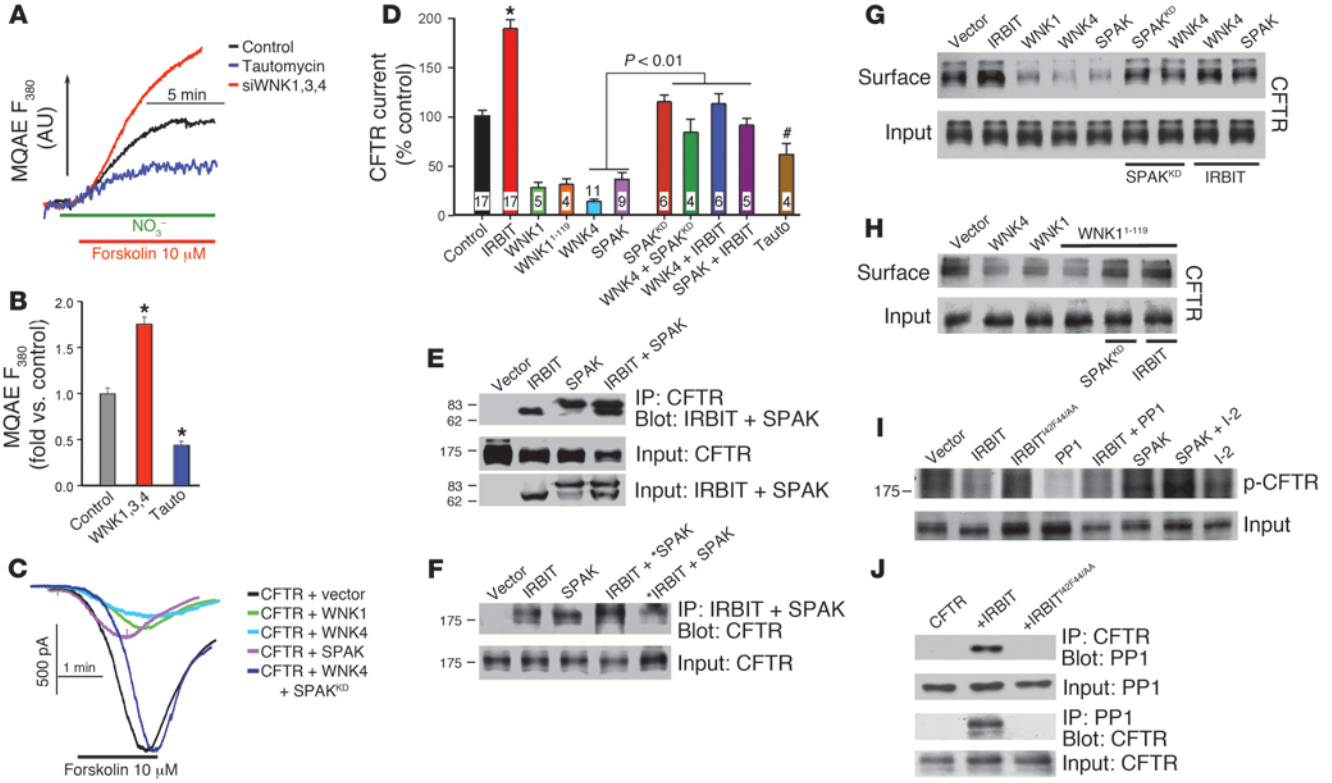

Figure 5

Regulation of CFTR by the WNK/SPAK and IRBIT/PP1 pathways. (**A** and **B**) Sealed ducts were treated with scrambled siRNA (black, blue) or WNK (red) siRNA and incubated for 5 minutes with 3 nM tautomycin (blue). CFTR activity was measured with MQAE as NO_3^-/Cl^- exchange activity. **B** shows mean ± SEM ($n = 3$, $^*P < 0.01$). (**C** and **D**) CFTR current was measured in HEK cells transfected with CFTR and the indicated IRBIT, WNK, and SPAK combinations or treated with 3 nM tautomycin for 5 minutes. **D** shows mean ± SEM ($n = 4$–17; $^*P < 0.01$; $^{\#}P < 0.05$ versus control). Currents were normalized to cell capacitance before averaging. (**E** and **F**) Mutual interaction of IRBIT and SPAK with CFTR, as measured by the reciprocal coimmunoprecipitation assays. In **F**, asterisks in lane 4 indicate expression of 4 times excess SPAK relative to IRBIT and in lane 5 expression of 4 times excess IRBIT relative to SPAK. (**G**) HEK cells expressing CFTR and the indicated combinations of IRBIT, WNK1, WNK4, and SPAK constructs were used to test their effect on surface expression of CFTR by biotinylation. (**H**) Inhibition of CFTR surface expression by WNK4, WNK1, and $WNK1^{1–119}$ and its reversal by $SPAK^{KD}$ and IRBIT. (**I**) HEK cells expressing CFTR and the indicated combinations of IRBIT, $IRBIT^{I42F44/AA}$, PP1, SPAK, and inhibitor-2 were used to measure CFTR phosphorylation, as described in Figure 3 for NBCe1-B. (**J**) HEK cells expressing CFTR and cotransfected with IRBIT or $IRBIT^{I42F44/AA}$ were used to show IRBIT-mediated recruitment of the native PP1 to CFTR. Averages for **G** and **H** are given in Supplemental Figure 4B and for **I** in Supplemental Figure 5B.

The WNK and SPAK kinases, PP1, and IRBIT in regulation of CFTR. The second limb of the fluid and HCO_3^- secretory pathway is luminal HCO_3^- exit mediated by the SLC26 transporters and CFTR. Therefore, in the next stage we used the tools in Figure 4G to ask whether the WNK/SPAK kinases act on CFTR and whether IRBIT/PP1 antagonizes the effect of the WNKs on CFTR expression and activity. CFTR and the SLC26 transporters were reported to be inhibited by the WNKs (25, 27). However, a recent study reported that at low cytoplasmic Cl^-, WNK1 phosphorylates SPAK, which then increases CFTR HCO_3^- permeability and inhibits the SLC26 transporters and CFTR-dependent HCO_3^- transport (26). Therefore, we used the probes in Figure 4G to clarify the regulation of CFTR by WNK/SPAK and IRBIT/PP1. The composite panels in Figure 5 show the results of these experiments. CFTR activity in the sealed pancreatic duct was measured by following intracellular Cl^- with the Cl^--sensitive dye MQAE, as reported previously (21). The ducts are bathed in medium in which NO_3^- replaces Cl^-. Exchange of intracellular Cl^- with extracellular NO_3^- ($Cl^-_{in}/NO_3^-_{out}$) by stimulated CFTR results in de-quenching of MQAE to report CFTR activity. Figure 5, A and B, shows that knockdown of the WNKs increases, whereas inhibition of PP1 inhibits, pancreatic duct CFTR activity.

Figure 5, C and D, shows that CFTR current measured in HEK cells transfected with CFTR is (a) activated by IRBIT and (b) inhibited by WNK1, WNK4, and SPAK and by inhibition of PP1 with tautomycin; (c) notably, CFTR is inhibited by $WNK1^{1–119}$, which lacks kinase function; (d) $SPAK^{KD}$ and IRBIT reverse the inhibition of CFTR by WNK4; and (e) IRBIT reverses inhibition of CFTR by SPAK. Hence, similar to the findings with NBCe1-B, the WNKs function as scaffolds for SPAK and SPAK inhibits CFTR Cl^- channel activity. The effect of the WNK/SPAK pathway is reversed by IRBIT, and this effect of IRBIT is mediated by PP1.

The effects of the WNK/SPAK and IRBIT/PP1 pathways can be accounted for by their effect on surface expression of CFTR. Thus, Figure 5, E and F, shows that SPAK and IRBIT interact with CFTR and their interactions are independent of each other. Figure 5G

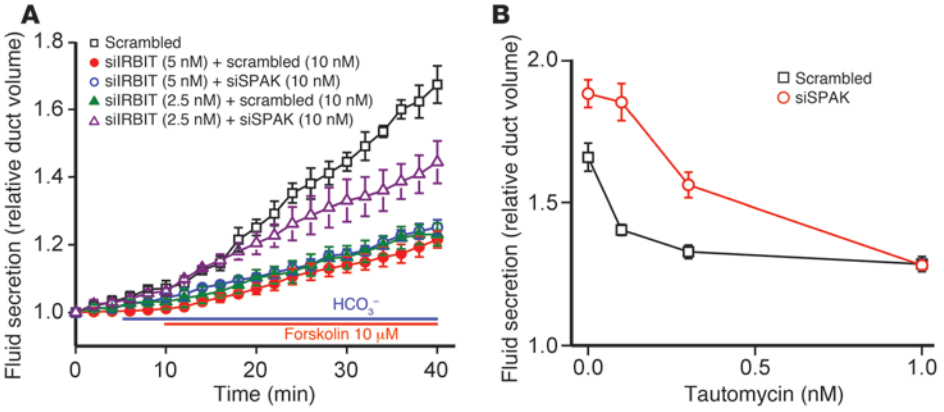

Figure 6
Physiological relevance of regulation of the WNK/SPAK pathway by the IRBIT/PP1 pathway. (**A**) Sealed pancreatic ducts were treated with 10 nM scrambled siRNA (black, red, and green traces), 5 nM IRBIT siRNA (red and blue traces), 2.5 nM IRBIT siRNA (green and purple traces), and 10 nM SPAK siRNA (blue and purple traces) and were used to measure stimulated ductal fluid secretion. (**B**) Sealed pancreatic ducts were treated with 10 nM scrambled (black trace) or SPAK siRNA (red trace). Ten minutes before and during the experiments, the ducts were treated with the indicated concentration of tautomycin, and fluid secretion was measured by video microscopy for 40 minutes. Results in **A** and **B** are mean ± SEM of 3–6 experiments.

shows that WNK1, WNK4, and SPAK reduce surface expression of CFTR, although WNK4 is somewhat more effective than WNK1; that $SPAK^{KD}$ reverses the effect of the WNKs; and that IRBIT reverses the effect of the WNKs and of SPAK on surface expression of CFTR. Moreover, Figure 5H shows that the WNK1 fragment $WNK1^{1–119}$ reduces surface expression of CFTR and the effect of $WNK1^{1–119}$ is reversed by $SPAK^{KD}$ and IRBIT ($n = 3$, $P < 0.01$; see Supplemental Figure 4). Figure 5I (^{32}P labeling assay) and Supplemental Figure 5B (assay with the anti–phospho-serine/threonine antibodies) show that IRBIT and PP1, but not $IRBIT^{I42F44/AA}$, reduce the phosphorylation of CFTR, whereas SPAK and inhibitor-2 increase the phosphorylation of CFTR. Finally, Figure 5J shows that IRBIT recruits PP1 to CFTR ($n = 3$, $P < 0.01$; see Supplemental Figure 5B).

Physiological relevance. The physiological relevance of regulation of ductal NBCe1-B and CFTR by IRBIT and PP1 is described in Figure 6, in which the relationship between regulation of fluid secretion by SPAK and IRBIT and SPAK and PP1 was examined. Treating sealed ducts with 5 nM IRBIT siRNA markedly inhibited fluid secretion, which could not be reversed even in part by cotreatment with SPAK siRNA. Reducing IRBIT siRNA to 2.5 nM to only partially knock down IRBIT was required to observe increased ductal fluid secretion by treatment with SPAK siRNA (Figure 6A). PP1 mediates the stimulatory effect of IRBIT, and the dominant effect of IRBIT and PP1 is demonstrated in Figure 6B, which shows that inhibition of PP1 with tautomycin strongly inhibited ductal fluid secretion. SPAK siRNA only shifted to the right the dose response for tautomycin.

Discussion

Transepithelial fluid and HCO_3^- secretion are critical for the survival of epithelia, as evident from the damage to all epithelial tissues in CF. Therefore, HCO_3^- secretion must be tightly regulated in the resting and stimulated state. The pancreatic duct is an excellent model to study the mechanism of fluid and HCO_3^- secretion, since it specializes in secreting a large volume of HCO_3^--rich fluid. Here, we report the relationship between two pathways that regulate ductal fluid and HCO_3^- secretion at rest and in the stimulated state. The pathways and the relationship between them are depicted in the model in Figure 7. Multiple probes were used to examine each component of the pathways in model systems and the in vivo sealed duct system. The overall findings indicate that the WNK kinases acting through SPAK have a major role in ductal function by stabilizing the resting state of ductal secretion. The WNKs do so by acting as scaffolds to recruit SPAK, which phosphorylates and inhibits the activity of the major

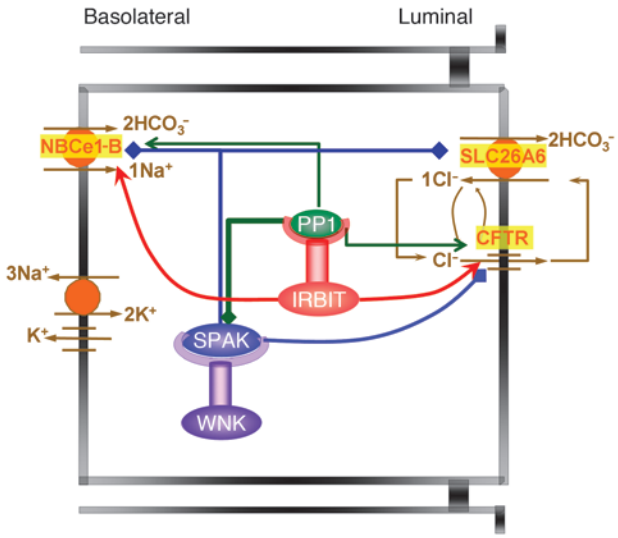

Figure 7
Regulation of ductal secretion by the WNK/SPAK and the IRBIT/PP1 pathways. The model shows that the WNK/SPAK pathway determines the duct resting secretory state by reducing NBCe1-B and CFTR surface expression and thus their activity. The WNKs are modeled to function as scaffolds for SPAK, and SPAK phosphorylates NBCe1-B and CFTR (blue lines). IRBIT determines the secretory state and dominates ductal secretion by both reversing the effect of the WNK/SPAK pathway and directly activating NBCe1-B and CFTR. IRBIT functions as a scaffold for PP1 to recruit PP1 to a complex with NBCe1-B and CFTR to dephosphorylate NBCe1-B and CFTR and restore their surface expression (green arrows). IRBIT then directly activates NBCe1-B and CFTR by preventing NBCe1-B autoinhibition by its N-terminal domain (24) and by interaction of the IRBIT PEST domain with CFTR (21). The dual effects of IRBIT, reversing the inhibitory state and stimulating the transporters, highlight the prominent role of IRBIT in epithelial fluid and electrolyte secretion.

ductal HCO_3^- transporters, NBCe1-B and CFTR, through the control of their surface expression. IRBIT dominates the secretory state by both antagonizing the effect of the WNK/SPAK pathway (demonstrated here) and directly stimulating NBCe1-B and CFTR (21, 24) to govern ductal secretion and stabilize the secretory state. IRBIT antagonizes the effect of the WNK/SPAK pathway by acting as a scaffold to recruit PP1, which dephosphorylates the HCO_3^- transporters and increases their surface expression. For simplicity and since it was not studied here, the potential effect of PP1 on SPAK phosphorylation (39) is not considered in the model. IRBIT then activates NBCe1-B by nullifying the inhibition of NBCe1-B by its cognate N-terminal inhibitory domain (24) and activates CFTR via its PEST domain (21).

The transport and regulatory scheme depicted in Figure 7 likely operates in other epithelia, since similar roles of the WNKs and IRBIT pathways are observed in the salivary duct, and the WNKs, IRBIT, and NBCe1-B are expressed in acinar cells (D. Yang and S. Muallem, unpublished observations). Furthermore, because of the multiple roles of the WNK kinases in epithelial physiology (3, 7, 11, 13), the finding that IRBIT is such a potent regulator of the WNK pathway likely has implications beyond fluid and electrolyte secretion in secretory glands. By reversing the inhibitory effect of the WNK/SPAK pathway, IRBIT likely has an important regulatory role in bodily volume regulation and blood pressure through regulation of renal ion transport, in acid-base regulation through regulation of HCO_3^- transporters, and in regulation of epithelial function through regulation of CFTR and NBCe1-B. This makes IRBIT a particularly attractive target for drug development to fine-tune the function of multiple organs that use ion transport to execute their major function.

Methods

Plasmid construction, materials, and solutions. CFTR, pNBC1, and IRBIT constructs were described previously (21). The WNK plasmids were described in refs. 12, 14. I-2/pCMV-neo was a gift from Anna DePaoli-Roach (Indiana University School of Medicine, Indianapolis, Indiana, USA), and pCDNA3/mPP1 was a gift from Eric Delpire (Vanderbilt University Medical Center, Nashville, Tennessee, USA). The cDNA encoding mSPAK (a gift from Melanie Cobb, University of Texas Southwestern Medical Center) was excised from the original vectors and transferred to p3xFLAG-CMV-7.1. Point mutations were generated by site-directed mutagenesis with a QuickChange kit (Stratagene). All constructs were verified by sequencing of the entire open reading frames. Tautomycin was obtained from Alexis Biochemicals. ^{32}P-orthophosphoric acid was from PerkinElmer. The standard bath solution (solution A) contained 140 mM NaCl, 5 mM KCl, 1 mM $MgCl_2$, 1 mM $CaCl_2$, 10 mM HEPES (pH 7.4 with NaOH), and 10 mM glucose. Na^+-free solutions were prepared by replacing Na^+ with *N*-methyl-D-glucamine (NMDG). HCO_3^--buffered solutions (solution B) were prepared by replacing 25 mM Na^+ salts with 25 mM Na^+-HCO_3^- and reducing HEPES to 2.5 mM. HCO_3^--buffered solutions were gassed with 5% CO_2 and 95% O_2. The osmolarity of all solutions was adjusted to 310 mosm with the major salt. The sources of antibodies were as follows: anti-GFP was from Invitrogen, anti-Flag was from Sigma-Aldrich, anti-CFTR was from Upstate, and anti-PP1 was from Santa Cruz Biotechnology Inc.

Isolation and culture of pancreatic and parotid ducts. All euthanasia procedures and experimental protocols with the mice followed NIH guidelines and were approved by the Animal Care and Use Committee of University of Texas Southwestern Medical Center. Cultured sealed pancreatic ducts were prepared by a modification of the procedure described by Ashton et al. (28). Sealed parotid ducts were prepared as described in ref. 37. In brief, female mice (20–25 g) were killed by cervical dislocation. The pancreas and parotid glands were removed and injected with a digestion buffer consisting of DMEM, containing 50 U/ml collagenase, 400 U/ml hyaluronidase, 0.2 mg/ml soybean trypsin inhibitor (STI), and 2 mg/ml BSA. The tissues were incubated at 37°C for 30 minutes and then in fresh digestion buffer for an additional 30 minutes. After one wash with DMEM containing 0.2 mg/ml STI and 3% (w/v) BSA, ducts were microdissected and cultured in DMEM supplemented with 10% fetal bovine serum at 37°C and, as indicated, treated with scrambled or the desired siRNA for 48–60 hours before use.

Treatment with siRNA and analysis of gene expression. siRNA treatment was as described previously (21, 29). The siRNA sequences used were siIRBIT, 5′-CAGAUACUAAUGGACAUAGUACAGT; siWNK1,3, 5′-UGUCAUUAGUUCAGUCACUdTdT; siWNK4, 5′-GGCAAGGGCUGACCACUAAGCAATC; siSPAK 5′-GGAACUUAAUGACAUACGAUUUGAG. Ducts were transfected within 1 hour after dissection and were kept in 35-mm dishes containing 2 ml DMEM with 10% FBS. Except in Figure 6, 100 pmol siRNA was diluted in 250 μl of Opti-MEM I, and 5 μl Lipofectamine 2000 was diluted in 250 μl of the same medium. The diluted siRNA and Lipofectamine 2000 were mixed and after 20 minutes were added to the dish. The final siRNA concentration was 10 nM. After 24 hours, the medium was replaced with fresh medium without the siRNA, and the ducts were cut in half to release the accumulated fluid and tension. The ducts were used 48–60 hours after the beginning of the transfection. In Figure 6 the amount of IRBIT siRNA was adjusted to obtain final concentrations of 5 and 2.5 nM. To assess efficiency of knockdown, total RNA was extracted from microdissected cultured sealed pancreatic ducts using RNeasy Mini Kit (QIAGEN). First-strand cDNA was synthesized with the SuperScript Preamplification System (Invitrogen). RT-PCR was performed with appropriate primers, with β-actin as a control cDNA.

Measurement of fluid secretion by the sealed ducts. Fluid secretion was measured by video microscopy. The sealed ducts were transferred to a perfusion chamber and perfused with HEPES- and then HCO_3^--buffered media and stimulated with 10 μM forskolin (Alomone). Images were captured every 2 minutes and analyzed offline by calculating the lumen volume as detailed before (21, 29). Due to the variation in size between the microdissected ducts, a normalization procedure was used, with the volume of the first image (V_0) set as 1.

Cell transfection. All transfections (HeLa and HEK cells) were with Lipofectamine 2000. Preliminary experiments were performed to determine the optimal transfection level. In particular, when the cells were transfected with multiple cDNAs, the transfection ratio was set in preliminary experiments, and the total cDNA was kept constant for all conditions with empty vector. When single transfected cells had to be identified, the cells were cotransfected with GFP. GFP fluorescence intensity was also used to select cells with similar expression level.

Intracellular pH, intracellular Cl^-, and Cl^- current measurements. Intracellular pH (pH_i) was measured with BCECF (Teflab) by recording BCECF fluorescence at excitation wavelengths of 490 and 440 nm and calibrating the fluorescence signals as before (21). Fluorescence was recorded from a section of the entire duct and clusters of 2–5 transfected HeLa cells (21). Ducts or HeLa cells loaded with BCECF were perfused with HEPES-buffered medium for at least 10 minutes before start of pH_i measurements. Na^+-HCO_3^- cotransport activity was initiated by acid load by perfusion with Na^+-free, HCO_3^--buffered medium containing 10 (ducts) or 2 (HeLa cells) μM EIPA to block Na^+/H^+ exchange activity and were then perfused with HCO_3^--buffered medium containing 140 mM Na^+. Na^+-HCO_3^- cotransport activity was estimated from the slope of changes in pH_i and normalized relative to controls that were included in every experiment.

For intracellular Cl^- measurement, the ducts were loaded with MQAE (Teflab) by incubation in DMEM supplemented with 10% fetal bovine

serum at 37°C containing 5 mM MQAE. After mounting, the ducts were washed, and MQAE fluorescence was recorded at an excitation wavelength of 360 nm. For measurement of Cl^- permeability, the ducts were exposed to solution A, in which Cl^- was replaced with NO_3^-, and were then stimulated with forskolin. The forskolin-stimulated Cl^-/NO_3^- exchange reports CFTR permeability. It is probable that the exchange in the sealed duct was made possible by luminal access of NO_3^- through the tight junctions.

Cl^- current was measured in HEK cells transfected with CFTR and empty vector (control) or the indicated IRBIT, WNK, and SPAK plasmids as detailed before (21, 29). In brief, the whole cell current was measured with pipette solution containing 150 mM NMDG-Cl, 1 mM $MgCl_2$, 1 mM EGTA, 0.5 mM ATP, and 10 mM HEPES at pH 7.3. The bath solution contained 150 mM NMDG-Cl, 1 mM $MgCl_2$, 1 mM $CaCl_2$, and 10 mM HEPES at pH 7.4. The pipettes had a resistance between 5 and 7 MΩ when filled with the pipette solution. Seal resistance was always more than 8 GΩ. Currents were recorded using the Axopatch 200B patch-clamp amplifier (Molecular Devices) at a holding potential of –60 mV, and results were collected at 5 kHz and filtered at 1 kHz. Currents were normalized to the cell capacitance before averaging.

Biotinylation and coimmunoprecipitation assays. Extracts were prepared by disruption of cells in ice-cold lysis buffer (20 mM Tris, 150 mM NaCl, 2 mM EDTA, 1% Triton X-100, and a protease inhibitor cocktail), incubation for 15–30 minutes, and collection by centrifugation. For biotinylation experiments, transfected HEK cells were incubated with 0.5 mg/ml EZ-LINK Sulfo-NHS-LC-Biotin (Thermo Scientific) for 30 minutes at 0°C, washed with PBS, and lysed as above. Biotinylated GFP–NBCe1-B and CFTR were isolated with avidin beads and recovered by heating at 37°C for 30 minutes. For coimmunoprecipitation, extracts were incubated with anti-GFP (Invitrogen) or anti-CFTR (M3A7; Upstate) antibodies. Beads were collected and washed 3 times with lysis buffer, and proteins were recovered by 30 minutes heating in SDS sample buffer at 60°C (GFP–NBCe1-B) or 37°C (CFTR).

In vivo phosphorylation. Two procedures were used to assay transporter phosphorylation, ^{32}P labeling and probing with anti-serine/threonine antibodies. For ^{32}P labeling, about 24 hours after transfection with NBCe1-B, CFTR and the indicated WNK, SPAK, IRBIT, and inhibitor-2 plasmids, HEK cells were starved for 18 hours in serum-free medium. Subsequently, the cells were washed with phosphate-free DMEM and labeled for 4 hours with 75 μCi/ml ^{32}P-orthophosphate. After labeling, the cells were washed 3 times with PBS and lysed. Lysates were immunoprecipitated with anti-GFP (Invitrogen) or anti-CFTR (M3A7; Upstate) antibodies. Samples were separated by 7.5% SDS-PAGE and transferred to a Whatman 3M paper, dried, and autoradiographed overnight at –80°C.

For probing with anti–phospho-serine/threonine antibodies, HEK293 cells were transiently transfected with NBCe1-B, CFTR, and the indicated WNK, SPAK, IRBIT, and inhibitor-2 plasmids. One day after transfection, cells were stimulated for 15 minutes with 50 μM forskolin and 5 mM 3-isobutylmethylxanthine. Lysates were incubated with anti-GFP (Invitrogen) and anti-CFTR (M3A7; Upstate) antibodies. Beads were collected and washed 3 times with lysis buffer, and proteins were recovered by heating and incubating in SDS sample buffer. Phospho-serine and phospho-threonine residues in proteins were detected by Anti-Phosphoserine/threonine (ECM Biosciences, Abcam).

Statistics. Results for all experiments are given as mean ± SEM of the indicated number of experiments. Significance was determined by ANOVA, and P values of less than 0.05 were considered significant.

Acknowledgments

We thank Anna DePaoli-Roach (Indiana University School of Medicine) for the gift of I-2/pCMV-neo. Eric Delpire (Vanderbilt University Medical Center, Nashville, Tennessee, USA) provided the plasmid coding PP1, and Melanie Cobb (University of Texas Southwestern Medical Center) provided the plasmid encoding mSPAK. This work was supported by an intramural grant from the NIDCR/Division of Intramural Research, NIH grants DE 12309 and DK076638, and a grant from the Cystic Fibrosis Foundation.

Received for publication April 25, 2010, and accepted in revised form December 15, 2010.

Address correspondence to: Shmuel Muallem, Epithelial Signaling and Transport Section, Molecular Physiology and Therapeutics Branch, NIDCR, Building 10, Room 1N-113, NIH, Bethesda Maryland 20892, USA. Phone: 301.402.0262; Fax: 301.402.1228; E-mail: shmuel.muallem@nih.gov.

1. Melvin JE, Yule D, Shuttleworth T, Begenisich T. Regulation of fluid and electrolyte secretion in salivary gland acinar cells. *Annu Rev Physiol*. 2005;67:445–469.
2. Steward MC, Ishiguro H, Case RM. Mechanisms of bicarbonate secretion in the pancreatic duct. *Annu Rev Physiol*. 2005;67:377–409.
3. Kahle KT, Ring AM, Lifton RP. Molecular physiology of the WNK kinases. *Annu Rev Physiol*. 2008; 70:329–355.
4. Dorwart MR, Shcheynikov N, Yang D, Muallem S. The solute carrier 26 family of proteins in epithelial ion transport. *Physiology (Bethesda)*. 2008;23:104–114.
5. Seidler U, et al. Knockout mouse models for intestinal electrolyte transporters and regulatory PDZ adaptors: new insights into cystic fibrosis, secretory diarrhoea and fructose-induced hypertension. *Exp Physiol*. 2009;94(2):175–179.
6. Rodan AR, Huang CL. Distal potassium handling based on flow modulation of maxi-K channel activity. *Curr Opin Nephrol Hypertens*. 2009;18(4):350–355.
7. Richardson C, Alessi DR. The regulation of salt transport and blood pressure by the WNK-SPAK/OSR1 signalling pathway. *J Cell Sci*. 2008; 121(pt 20):3293–3304.
8. Huang CL, Cha SK, Wang HR, Xie J, Cobb MH. WNKs: protein kinases with a unique kinase domain. *Exp Mol Med*. 2007;39(5):565–573.
9. Xu B, English JM, Wilsbacher JL, Stippec S, Goldsmith EJ, Cobb MH. WNK1, a novel mammalian serine/threonine protein kinase lacking the catalytic lysine in subdomain II. *J Biol Chem*. 2000; 275(22):16795–16801.
10. Wilson FH, et al. Human hypertension caused by mutations in WNK kinases. *Science*. 2001; 293(5532):1107–1112.
11. Deaton SL, Sengupta S, Cobb MH. WNK kinases and blood pressure control. *Curr Hypertens Rep*. 2009; 11(6):421–426.
12. He G, Wang HR, Huang SK, Huang CL. Intersectin links WNK kinases to endocytosis of ROMK1. *J Clin Invest*. 2007;117(4):1078–1087.
13. Huang CL, Yang SS, Lin SH. Mechanism of regulation of renal ion transport by WNK kinases. *Curr Opin Nephrol Hypertens*. 2008;17(5):519–525.
14. Wang HR, Liu Z, Huang CL. Domains of WNK1 kinase in the regulation of ROMK1. *Am J Physiol Renal Physiol*. 2008;295(2):F438–F445.
15. Gagnon KB, England R, Delpire E. Characterization of SPAK and OSR1, regulatory kinases of the Na-K-2Cl cotransporter. *Mol Cell Biol*. 2006;26(2):689–698.
16. Durie PR. The pathophysiology of the pancreatic defect in cystic fibrosis. *Acta Paediatr Scand Suppl*. 1989; 363:41–44.
17. Ko SB, et al. Corticosteroids correct aberrant cystic fibrosis transmembrane conductance regulator localization in the duct and regenerate acinar cells in autoimmune pancreatitis. *Gastroenterology*. 2010; 138(5):1988–1996.
18. Almstahl A, Wikstrom M. Electrolytes in stimulated whole saliva in individuals with hyposalivation of different origins. *Arch Oral Biol*. 2003;48(5):337–344.
19. Abuladze N, et al. Molecular cloning, chromosomal localization, tissue distribution, and functional expression of the human pancreatic sodium bicarbonate cotransporter. *J Biol Chem*. 1998; 273(28):17689–17695.
20. Boron WF, Chen L, Parker MD. Modular structure of sodium-coupled bicarbonate transporters. *J Exp Biol*. 2009;212(pt 11):1697–1706.
21. Yang D, et al. IRBIT coordinates epithelial fluid and HCO3– secretion by stimulating the transporters pNBC1 and CFTR in the murine pancreatic duct. *J Clin Invest*. 2009;119(1):193–202.
22. Ando H, Mizutani A, Kiefer H, Tsuzurugi D, Michikawa T, Mikoshiba K. IRBIT suppresses IP3 receptor activity by competing with IP3 for the common binding site on the IP3 receptor. *Mol Cell*. 2006; 22(6):795–806.
23. Ando H, Mizutani A, Matsu-ura T, Mikoshiba K. IRBIT, a novel inositol 1,4,5-trisphosphate (IP3) receptor-binding protein, is released from the IP3 receptor upon IP3 binding to the receptor. *J Biol Chem*. 2003;278(12):10602–10612.
24. Shirakabe K, et al. IRBIT, an inositol 1,4,5-trisphosphate receptor-binding protein, specifically binds to and activates pancreas-type Na+/HCO3–

cotransporter 1 (pNBC1). *Proc Natl Acad Sci U S A*. 2006;103(25):9542–9547.
25. Kahle KT, et al. WNK4 regulates apical and basolateral Cl– flux in extrarenal epithelia. *Proc Natl Acad Sci U S A*. 2004;101(7):2064–2069.
26. Park HW, et al. Dynamic regulation of CFTR bicarbonate permeability by [Cl–]i and its role in pancreatic bicarbonate secretion. *Gastroenterology*. 2010; 139(2):620–631.
27. Yang CL, et al. WNK1 and WNK4 modulate CFTR activity. *Biochem Biophys Res Commun*. 2007; 353(3):535–540.
28. Ashton N, Argent BE, Green R. Effect of vasoactive intestinal peptide, bombesin and substance P on fluid secretion by isolated rat pancreatic ducts. *J Physiol*. 1990;427:471–482.
29. Wang Y, et al. Slc26a6 regulates CFTR activity in vivo to determine pancreatic duct HCO3– secretion: relevance to cystic fibrosis. *EMBO J*. 2006; 25(21):5049–5057.
30. Choate KA, Kahle KT, Wilson FH, Nelson-Williams C, Lifton RP. WNK1, a kinase mutated in inherited hypertension with hyperkalemia, localizes to diverse Cl– -transporting epithelia. *Proc Natl Acad Sci U S A*. 2003;100(2):663–668.
31. Welling PA, Chang YP, Delpire E, Wade JB. Multigene kinase network, kidney transport, and salt in essential hypertension. *Kidney Int*. 2010;77(12):1063–1069.
32. Devogelaere B, et al. Protein phosphatase-1 is a novel regulator of the interaction between IRBIT and the inositol 1,4,5-trisphosphate receptor. *Biochem J*. 2007;407(2):303–311.
33. MacKintosh C, Klumpp S. Tautomycin from the bacterium Streptomyces verticillatus. Another potent and specific inhibitor of protein phosphatases 1 and 2A. *FEBS Lett*. 1990;277(1–2):137–140.
34. Fernandez-Salazar MP, et al. Basolateral anion transport mechanisms underlying fluid secretion by mouse, rat and guinea-pig pancreatic ducts. *J Physiol*. 2004;556(pt 2):415–428.
35. Ishiguro H, Steward MC, Lindsay AR, Case RM. Accumulation of intracellular HCO3– by Na(+)-HCO3– cotransport in interlobular ducts from guinea-pig pancreas. *J Physiol*. 1996;495(pt 1):169–178.
36. Zhao H, Star RA, Muallem S. Membrane localization of H+ and HCO3– transporters in the rat pancreatic duct. *J Gen Physiol*. 1994;104(1):57–85.
37. Shcheynikov N, et al. The Slc26a4 transporter functions as an electroneutral Cl–/I–/HCO3– exchanger: role of Slc26a4 and Slc26a6 in I– and HCO3– secretion and in regulation of CFTR in the parotid duct. *J Physiol*. 2008;586(16):3813–3824.
38. Picking WD, et al. Fluorescence studies on the interaction of inhibitor 2 and okadaic acid with the catalytic subunit of type 1 phosphoprotein phosphatases. *Biochemistry*. 1991;30(42):10280–10287.
39. Gagnon KB, Delpire E. Multiple pathways for protein phosphatase 1 (PP1) regulation of Na-K-2Cl cotransporter (NKCC1) function: the N-terminal tail of the Na-K-2Cl cotransporter serves as a regulatory scaffold for Ste20-related proline/alanine-rich kinase (SPAK) AND PP1. *J Biol Chem*. 2010; 285(19):14115–14121.